ORGANOMETALLICS

Article

pubs.acs.org/Organometallics

CF_3–Ph Reductive Elimination from [(Xantphos)Pd(CF_3)(Ph)]

Vladimir I. Bakhmutov,*[,§] Fernando Bozoglian,[†] Kerman Gómez,[†] Gabriel González,[†] Vladimir V. Grushin,*[,†] Stuart A. Macgregor,*[,‡] Eddy Martin,[†] Fedor M. Miloserdov,[†] Maxim A. Novikov,[†] Julien A. Panetier,[‡] and Leonid V. Romashov[†]

[†]The Institute of Chemical Research of Catalonia (ICIQ), Tarragona 43007, Spain

[‡]School of Engineering and Physical Sciences, William H. Perkin Building, Heriot-Watt University, Edinburgh EH14 4AS, U.K.

[§]Department of Chemistry, Texas A&M University, College Station, Texas 77842, United States

Supporting Information

ABSTRACT: CF_3–Ph reductive elimination from [(Xantphos)Pd(Ph)(CF_3)] (**1**) and [(*i*-Pr-Xantphos)Pd(Ph)(CF_3)] (**2**) has been studied by experimental and computational methods. Complex **1** is cis in the solid state and predominantly cis in solution, undergoing degenerate cis–cis isomerization ($\Delta G^{\neq}_{exp}$ = 13.4 kcal mol^{-1}; $\Delta G^{\neq}_{calc}$ = 12.8 kcal mol^{-1} in toluene) and slower cis–trans isomerization (ΔG_{calc} = +0.9 kcal mol^{-1}; $\Delta G^{\neq}_{calc}$ = 21.9 kcal mol^{-1}). In contrast, **2** is only trans in both solution and the solid state with **trans-2** computed to be 10.2 kcal mol^{-1} lower in energy than **cis-2**. Kinetic and computational studies of the previously communicated (*J. Am. Chem. Soc.* **2006**, *128*, 12644), remarkably facile CF_3–Ph reductive elimination from **1** suggest that the process does not require P–Pd bond dissociation but rather occurs directly from **cis-1**. The experimentally determined activation parameters ($\Delta H^{\neq}$ = 25.9 ± 2.6 kcal mol^{-1}; $\Delta S^{\neq}$ = 6.4 ± 7.8 e.u.) are in excellent agreement with the computed data ($\Delta H^{\neq}_{calc}$ = 24.8 kcal mol^{-1}; $\Delta G^{\neq}_{calc}$ = 25.0 kcal mol^{-1}). $\Delta G^{\neq}_{calc}$ for CF_3–Ph reductive elimination from **cis-2** is only 24.0 kcal mol^{-1}; however, the overall barrier relative to **trans-2** is much higher ($\Delta G^{\neq}_{calc}$ = 34.2 kcal mol^{-1}) due to the need to include the energetic cost of trans–cis isomerization. This is consistent with the higher thermal stability of **2** that decomposes to $PhCF_3$ only at 100 °C and even then only in a sluggish and less selective manner. The presence of excess Xantphos has a minor decelerating effect on the decomposition of **1**. A steady slight decrease in k_{obs} in the presence of 1 and 2 equiv of Xantphos then plateaus at [Xantphos]:**1** = 5, 10, and 20. Specific molecular interactions between **1** and Xantphos are not involved in this kinetic effect (NMR, T_1 measurements). A deduced kinetic scheme accounting for the influence of extra Xantphos involves the formation of *cis*-[(η^1-Xantphos)$_2$Pd(Ph)(CF_3)] that, by computation, is predicted to access reductive elimination of CF_3–Ph with $\Delta G^{\neq}_{calc}$ = 22.8 kcal mol^{-1}.

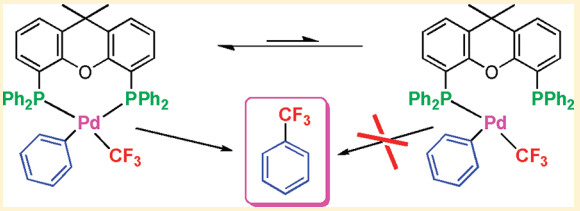

INTRODUCTION

Selectively fluorinated aromatic compounds are widely used as building blocks and intermediates in the synthesis of pharmaceuticals, agrochemicals, and specialty materials.[1] Of particular interest are derivatives bearing trifluoromethyl groups on the aromatic ring.[1−7] These important compounds are manufactured via a Swarts-type process involving exhaustive chlorination of a methyl group on the ring, followed by Cl/F exchange on the trichloromethyl product with HF.[8] In this process, 3 equiv of Cl_2 are consumed and 6 equiv of HCl are formed for each equivalent of the desired products that is produced. An alternative to this eco-unfriendly method would be highly efficient metal-catalyzed cross-coupling of aromatic electrophiles, such as haloarenes with an inexpensive nucleophilic CF_3 source. Such reactions employing stoichiometric amounts of copper are well-known,[2−7] and more recently, catalytic versions of this transformation were developed.[9] However, the copper-promoted/catalyzed reactions only readily occur with costly iodoarenes, whereas cheaper aryl bromides and chlorides are much less reactive toward Cu-CF_3 reagents.[7] In contrast, palladium is able to mediate cross-coupling reactions with Ar-Br and Ar-Cl substrates, and so the extension of these methods to Pd-catalyzed aromatic trifluoromethylation has been highly sought after.

The intrinsic problem with nucleophilic aromatic trifluoromethylation, catalyzed by palladium, is the exceptional strength and inertness of the Pd–CF_3 bond: even at high temperatures (135–145 °C), the CF_3–Ar reductive elimination step either does not occur at all[10] or is sluggish and poorly selective.[11] In sharp contrast, analogous nonfluorinated complexes reductively eliminate toluene at as low as 15–40 °C.[12] In 2006, an important result for the area was reported,[13,14] showing that [(Xantphos)Pd(Ph)(CF_3)] undergoes clean and facile CF_3–Ph reductive elimination at as low as 50–80 °C (eq 1). This finding demonstrated, for the first time, the very possibility of Pd-catalyzed trifluoromethylation of aryl halides. Indeed, in 2010, the first trifluoromethylation of chloroarenes, catalytic in Pd-BrettPhos (or RuPhos), was

Special Issue: Fluorine in Organometallic Chemistry

Received: October 14, 2011
Published: December 28, 2011

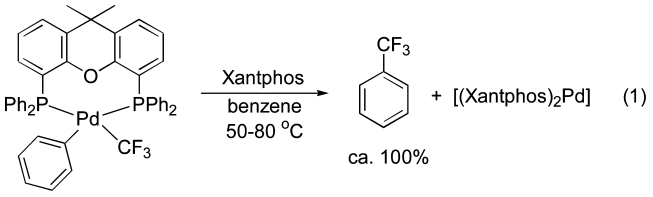

(1)

reported by Buchwald's group.[15] They also performed a computational and kinetic study on [(BrettPhos)Pd(Ar)(CF_3)] to show that Pd−CF_3 bond cleavage is the main contributor to the activation barrier to reductive elimination.

Only three ligands are currently known that promote CF_3−Ar reductive elimination from Pd(II):[16] Xantphos, BrettPhos, and RuPhos. To find other, less expensive ligands for Pd-catalyzed aromatic trifluoromethylation, a detailed mechanistic understanding of CF_3−Ar bond formation at Pd(II) is desirable. Herein, we report a combined experimental and computational study of the CF_3−Ph reductive elimination from [(Xantphos)Pd(Ph)(CF_3)] (**1**), the first reported complex[13] to cleanly and readily undergo this transformation.

EXPERIMENTAL STUDIES

Synthesis and Characterization of [(Xantphos)Pd(Ph)(CF_3)] and [(*i*-Pr-Xantphos)Pd(Ph)(CF_3)]. The previously developed procedure[13] was used to synthesize **1** via treatment of [(Xantphos)Pd(Ph)(F)] (prepared in situ) with Ruppert's reagent, CF_3SiMe_3. The fluoride complex was made by our originally developed method involving ultrasound-promoted Pd-I/AgF exchange.[17] When a newly purchased batch of AgF (Aldrich, 99.9% trace metals basis, Lot no. MKBB6837) was used to react with [(Xantphos)Pd(Ph)(I)],[13] the primary product [(Xantphos)Pd(Ph)(F)] and eventually **1** prepared from it were contaminated with a dark material. This suggested[17b] that the new AgF reagent contained more water[18] than the one used in the original work.[13] It has been previously shown[17b] that the H_2O-induced Pd(II)/P(III) to Pd(0)/P(V) redox process readily occurring under the reaction conditions produces deeply colored Pd(0) species that stain the palladium fluoride product. Indeed, after the AgF reagent (5 mg) was sonicated in rigorously dry C_6D_6 (99% D, 0.6 mL) for 3 h, a peak from water at 0.5 ppm appeared in the ^{1}H NMR spectrum of the sample. Integration of the water signal against the residual solvent peak allowed the lower limit of the water content in the AgF reagent to be estimated at ca. 0.3 mol %.

The staining problem emerging from the presence of excessive water in some AgF samples can be solved by our previously developed[17b] technique. Indeed, when the reaction of [(Xantphos)Pd(Ph)(I)] with the new AgF reagent was repeated in the presence of 5 mol % PhI and 5 mol % Xantphos, the solution of [(Xantphos)Pd(Ph)(F)] produced was not nearly as dark after filtration. On treatment of this solution with CF_3SiMe_3, **1** was formed and isolated pure as well-shaped, pale yellow crystals in 60−85% yield, as previously communicated.[13]

Although cis in the crystal, complex **1** exists as a mixture of cis and trans isomers in solution.[13] As expected, the cis-to-trans ratio is solvent-dependent, being ca. 10:1 in benzene or toluene, >20:1 in THF, and >50:1 in CH_2Cl_2. Although the equilibrium between **cis-1** and **trans-1** establishes within the time of dissolution, there is no fast exchange on the NMR time scale between the two isomers at 25 °C. This is clearly indicated by sharp, well-resolved ^{19}F and ^{31}P resonances from the less-populated trans isomer. Despite that, broadened ^{19}F and ^{31}P NMR signals are always observed from the major, cis isomer of **1** at room temperature (Figures S1−S6, Supporting Information). On cooling a solution of **1** in CD_2Cl_2 to 0 °C, the ^{31}P resonances from **cis-1** appeared as 1:1 well-resolved doublets of quartets at 8.4 ppm (P trans to CF_3; J_{P-F} = 48 Hz, J_{P-P} = 22 Hz) and 12.6 ppm (P cis to CF_3; J_{P-F} = 8 Hz, J_{P-P} = 22 Hz). In THF, however, slightly less well-resolved ^{31}P NMR multiplets for **cis-1** could only be observed at a much lower temperature, −40 °C. Analysis of the VT NMR spectra of **1** in THF, toluene, and CD_2Cl_2 (Figures S1−S6, Supporting Information) showed that the temperature evolution of the ^{19}F and ^{31}P signals is typical of P−P exchange leading to averaging of the P sites on the NMR time scale. The observed temperature dependence of the ^{31}P line shapes originates from a multicenter exchange that is difficult to treat quantitatively. Therefore, line-shape analysis of the spectra was performed in approximation for a two-site exchange with the splitting of the signals from the ^{31}P−^{31}P and ^{31}P−^{19}F spin−spin coupling replaced by the correspondingly increased resonance widths. ^{31}P line-shape simulations by a conventional computer program produced exchange rate constants and free energy values for degenerate **cis-1** to **cis-1** isomerization (Table 1). As can be seen, these parameters show only a slight solvent dependence. In the absence of fast (on the NMR time scale) Pd−P dissociation, a much slower process, the degenerate isomerization of **cis-1** likely proceeds via a trigonal transition state (see below). The nondegenerate cis−trans isomerization of **1** occurs with a higher energy barrier, as follows from the NMR data.

Table 1. Rate Constants and $\Delta G^{\neq}$ Values (25 °C) for Degenerate cis-1 to cis-1 Isomerization in Different Solvents As Derived from ^{31}P NMR Line-Shape Analysis

solvent	k_{exch}, s^{-1}	$\Delta G^{\neq}$, kcal mol^{-1}
THF	909	13.0
toluene	417	13.4
CD_2Cl_2	86	14.3

We have also synthesized an analogue of **1** bearing isopropyl groups on the phosphorus centers, [(*i*-Pr-Xantphos)Pd(Ph)(CF_3)] (**2**; *i*-Pr-Xantphos = 4,5-bis(diisopropylphosphino)-9,9-dimethylxanthene). The desired precursor for the synthesis of **2**, [(*i*-Pr-Xantphos)Pd(Ph)(Br)], was not produced upon treatment of Pd_2dba_3 with PhBr in the presence of *i*-Pr-Xantphos in benzene or toluene.[19] Ligand exchange between [(Ph_3P)$_2$Pd(Ph)(Br)] and *i*-Pr-Xantphos in THF or benzene gave **2** in high yield, but even when *i*-Pr-Xantphos was used in 30% excess, the starting complex [(Ph_3P)$_2$Pd(Ph)(Br)] was still present (6−10%) in the reaction mixture at equilibrium (^{31}P NMR). Although attempts to isolate pure [(*i*-Pr-Xantphos)Pd(Ph)(Br)] in the bulk failed, we were able to characterize this species by single-crystal X-ray diffraction (Figure 1) and also in solution by ^{1}H and ^{31}P NMR.[20] It was found, however, that **2** can be easily made by reacting [(Ph_3P)$_2$Pd(Ph)(Br)] with *i*-Pr-Xantphos in THF, followed by treatment of the equilibrated mixture with CF_3SiMe_3/CsF (eq 2). Note that **1** could not be prepared this way from [(Xantphos)Pd(Ph)(I)] because of the facile and irreversible displacement of Xantphos by "CF_3^-" that is uncontrollably released from CF_3SiMe_3/F^-.[13] This is a clear indication that, as expected, more electron-rich *i*-Pr-Xantphos binds more tightly to Pd than Xantphos.

dx.doi.org/10.1021/om200985g | *Organometallics* 2012, 31, 1315−1328

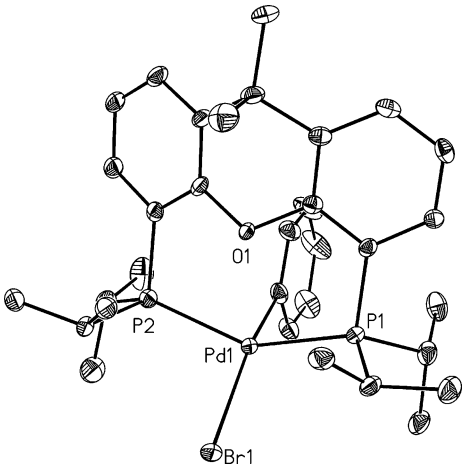

Figure 1. ORTEP drawing of [(*i*-Pr-Xantphos)Pd(Ph)(Br)] with thermal ellipsoids drawn to the 50% probability level and all H atoms omitted for clarity.

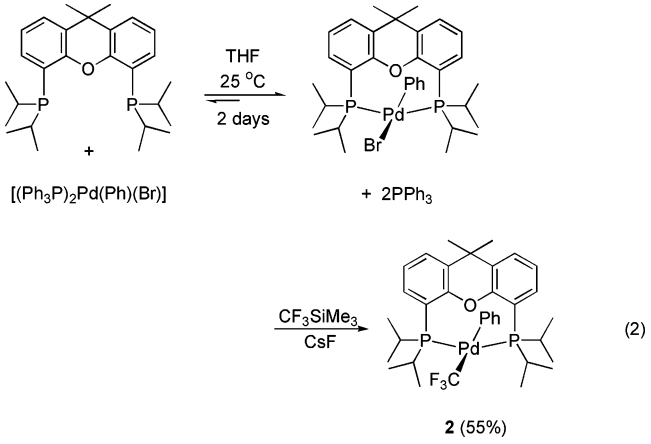

Complex **2** is air- and moisture-stable. Unlike **1**, which is cis in the solid state and predominantly cis in solution,[13] **2** bearing bulkier isopropyl groups on the P atoms is exclusively trans both in the crystal (Figure 2) and in solution. The Pd atom in **2**

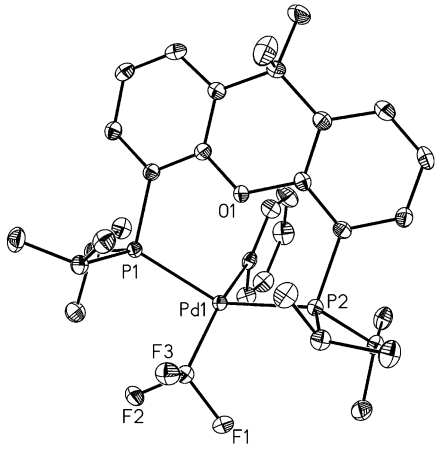

Figure 2. ORTEP drawing of **2** with thermal ellipsoids drawn to the 50% probability level and all H atoms omitted for clarity.

is very crowded, as follows from the appearance of four ^{1}H NMR signals from the nonequivalent methyl groups of the isopropyl substituents. Furthermore, all five protons of the *σ*-phenyl ligand are nonequivalent as well, appearing as separate resonances and suggesting hindered rotation around the Pd–Ph bond. On the other hand, the ^{19}F and ^{31}P NMR signals from **2** appear as well-resolved multiplets, a triplet (−13.1 ppm) and a quartet (20.0 ppm), respectively, with J_{P-F} = 13.8 Hz, pointing to free rotation around the Pd–CF_3 bond.

Complex **2** appeared to be less prone to CF_3–Ph reductive elimination than **1**. No reaction was observed after **2** was heated in toluene at 80 °C overnight, whereas **1** undergoes full decomposition to $PhCF_3$ at this temperature within a few hours.[13] After 3 days at 100 °C, **2** was decomposed to 80–90% conversion with only ca. 50–60% selectivity to $PhCF_3$ (^{19}F NMR). Therefore, the CF_3–Ph bond formation was studied in detail only for complex **1**.

Kinetic Studies of the Formation of $PhCF_3$ from [(Xantphos)Pd(Ph)(CF_3)]. Two general pathways could be considered for the formation of $PhCF_3$ from **1** (Scheme 1). In

Scheme 1

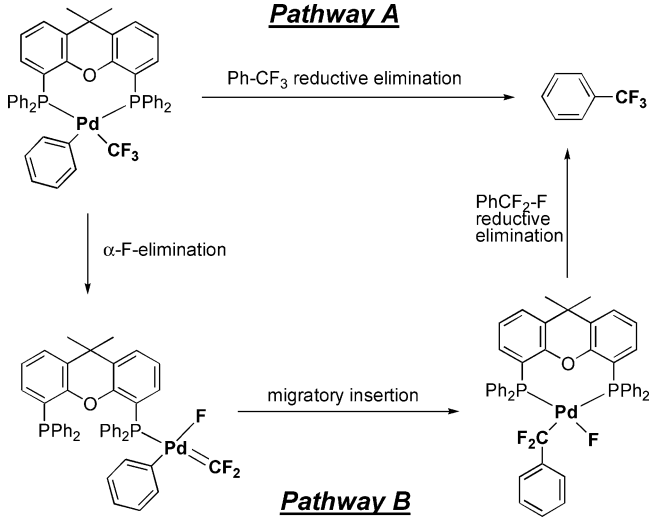

addition to direct CF_3–Ph reductive elimination (Pathway A), one could imagine another, indirect route leading to the same product (Pathway B). This other proposed pathway involves *α*-fluorine elimination, followed by migratory insertion of the resultant difluorocarbene into the Pd–Ph bond and subsequent $PhCF_2$–F reductive elimination. Indeed, *α*-fluorine elimination is well known for late-transition-metal complexes bearing CF_3 ligands,[21−23] palladium included.[11] Furthermore, migratory insertion within a $CH_3Pt{=}CF_2$ moiety to give the corresponding $PtCF_2CH_3$ species has been observed.[24] Finally, closely related reductive elimination of PhCOF from [$(Ph_3P)_2$Pd(PhCO)(F)] has been reported[17a,14,25] to easily occur even below room temperature.

The involvement of Pathway B could be examined by carrying out the decomposition of **1** in the presence of water because dihalocarbene complexes are instantaneously hydrolyzed to carbonyl species.[21a,23] If the latter carries a *σ*-aryl ligand on Pd, CO migratory insertion should easily occur, followed by a series of reductive elimination processes leading to aromatic carbonyl compounds, such as $(ArCO)_2O$, ArCOF, and ArCOOH.[11] The decomposition of **1** in toluene–water at 60 °C, in the absence or in the presence of extra Xantphos (2 equiv), produced $PhCF_3$ in high yield (^{19}F NMR). Benzoic acid derivatives PhCOX (X = F, OH, PhCOO), however, were not

dx.doi.org/10.1021/om200985g | *Organometallics* 2012, 31, 1315–1328

detected (^{19}F NMR, GC-MS), which prompted us to exclude Pathway B from further considerations.

To gain insight into the mechanism of reaction 1, the kinetics of the thermal decomposition of **1** in toluene were studied by ^{19}F NMR. In the absence of extra Xantphos, the reaction produced $PhCF_3$ along with palladium black and [(Xantphos)$_2$Pd] emerging from disproportionation of unstable [(Xantphos)Pd] that is co-formed in the reductive elimination process (Scheme 2).

Scheme 2

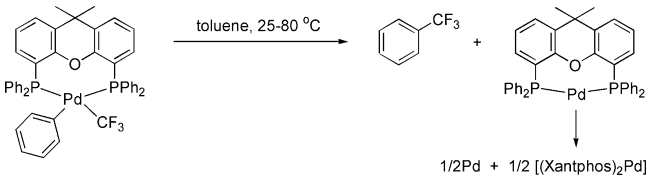

The reaction proceeded with high selectivity toward the formation of $PhCF_3$ and displayed first-order kinetics. Measuring the rate constants with experimental error of ca. 15% in the temperature range from +50 to +80 °C allowed for the determination of the activation parameters: $\Delta H^{\neq}$ = 25.9 ± 2.6 kcal mol^{-1} and $\Delta S^{\neq}$ = 6.4 ± 7.8 e.u. Despite the modest accuracy in the determination of the activation entropy, the value obtained points to participation of one molecule of **1** in the kinetically controlled step of the process. The reaction was found to be twice as slow in THF as in toluene at 60 °C. However, activation parameters in THF could not be determined because of the narrow temperature window available for this solvent (bp = 66 °C). In the kinetic runs in toluene, the selectivity of the reaction was either >90% (at 50, 60, and 70 °C) or near to 90% (80 °C), indicating that the simultaneous decomposition of the byproduct [(Xantphos)Pd], an unstable zerovalent palladium complex, did not interfere significantly with the CF_3–Ph bond-forming process. It is worth noting, however, that, in accord with the previously reported data,[13] the reaction was nearly 100% selective in the entire temperature range when performed in the presence of extra Xantphos to stabilize the [(Xantphos)Pd] in the form of [(Xantphos)$_2$Pd]. Therefore, a kinetic study of the reaction in the presence of extra Xantphos was also carried out.

The reaction of **1** in the presence of Xantphos that is also consumed (eq 1) exhibited first-order kinetics. A series of rate measurement experiments revealed that Xantphos had a small, yet reproducible, effect on the rate of the thermal decomposition of **1**. At 70 °C, k_{obs} decreased from 6.4 × 10^{-3} min^{-1} to 5.5 × 10^{-3} and 4.6 × 10^{-3} min^{-1} in the presence of 1 and 2 equiv of added Xantphos, respectively. The effect then plateaued at k_{obs} = ca. 4.3 × 10^{-3} min^{-1} in the presence of 5, 10, and 20 equiv of Xantphos. The positive, nonzero y intercept on the plot of k_{obs} vs [Xantphos]$^{-1}$ (Figure S10, Supporting Information) suggested that reaction 1 might proceed via two mechanistic pathways with similar barriers, one of which is suppressed by an extra ligand. In principle, the extra Xantphos effect might also be caused by (i) catalysis of the reaction with some species that are sequestered by Xantphos or (ii) changes in properties of the medium in the vicinity of **1** in the presence of Xantphos and/or by specific interactions between **1** and Xantphos. In addition, wide bite angle diphosphines can also change their coordination mode from η^2 to η^1, as shown in Scheme 3,[27,28] and this may also

Scheme 3

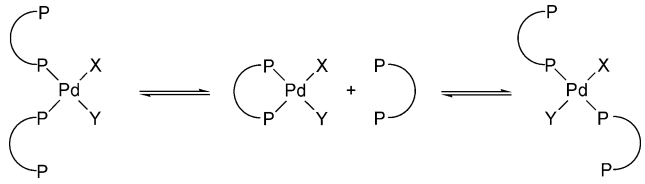

potentially affect the rate of reductive elimination from the metal center. Whatever the reason, the observed effect of an extra ligand contrasts the reported[26] lack of influence of added Xantphos on the rate of reductive elimination of *N*-aryl amidates from Xantphos-stabilized Pd(II).

Possible interactions between **1** and Xantphos were probed by ^{19}F and ^{31}P NMR analysis of **1** in the presence of a large excess of Xantphos. This experiment was carried out in CD_2Cl_2 because of the insufficient solubility of **1** in toluene and benzene and of Xantphos in THF. The addition of 20 equiv of Xantphos to a solution of **1** in CD_2Cl_2 ([**1**] = 2 × 10^{-2} M) resulted in the appearance of new, very low intensity signals in the NMR spectra. The signals were registered approximately 10 min (^{19}F) and 30 min (^{31}P) after the NMR sample was prepared. In the ^{19}F NMR spectrum, a triplet emerged at −19.7 ppm with J_{P-F} = 24 Hz. In the ^{31}P NMR spectrum, a quartet at 16.1 ppm with the same coupling constant (J_{P-F} = 24 Hz) and a singlet of the same integral intensity at −19.5 ppm were detected. These resonances were consistent with the structure of *trans*-[(η^1-Xantphos)$_2$Pd(Ph)(CF$_3$)], the cis isomer being not detected. We, therefore, reasoned that [(η^1-Xantphos)$_2$Pd(Ph)(CF$_3$)] was produced as a result of an equilibrium between **1** and Xantphos, as shown in eq 3. Integration of the new

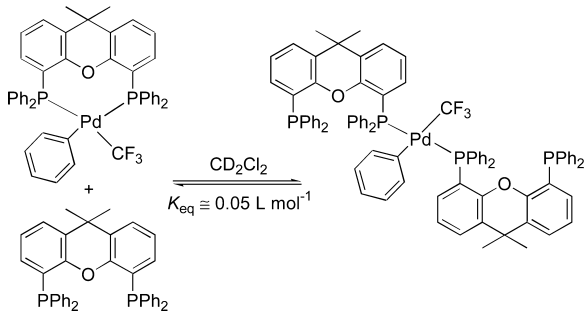

(3)

signals against those from **1** allowed for the determination of the molar ratio of *trans*-[(η^1-Xantphos)$_2$Pd(Ph)(CF$_3$)] to **1** at ca. 1:50. On the basis of these data, K_{eq} for reaction 3 was estimated at ca. 5 × 10^{-2} L mol^{-1}. Importantly, the triplet at −19.7 ppm with J_{P-F} = 24 Hz was also observed in the kinetic runs in the presence of extra Xantphos. Reliable quantification of the appearance and disappearance of this resonance in the kinetic runs was precluded by its low intensity.

Specific molecular interactions between **1** and Xantphos might change the nature of the medium in the vicinity of the complex, leading to a decrease in conformational mobility of **1** and thereby affecting the rate of the reductive elimination. To explore this hypothesis, we measured spin–lattice relaxation times[29] for the P nuclei in Xantphos alone, in **1** alone, and in a 2:1 mixture of Xantphos and **1** in toluene-d_8 at ambient temperature (Table 2). In all these measurements, the concentrations were maintained at the levels used for the kinetic studies. The data indicate that the T_1 time of the P nuclei in the free ligand was not affected by the presence of **1**

dx.doi.org/10.1021/om200985g | *Organometallics* 2012, 31, 1315–1328

Table 2. Spin−Lattice Relaxation Times (T_1) of Xantphos, 1, and Their Mixtures in Toluene-d_8 at 25 °C

	T_1, sec		
sample	Xantphos	cis-1	trans-1
Xantphos (0.14 M)	9.3		
1 (0.07 M)		4.0	3.2
Xantphos (0.14 M) + 1 (0.07 M)	9.1	10.7	6.3

(9.3 vs 9.1 s)[30] and points to a lack of interaction between **1** and Xantphos occurring rapidly on the NMR time scale. We can, therefore, rule out any influence of such interactions on the rate of reductive elimination from **1**.

Taken together, our observations on the experimentally detected extra Xantphos effect indicate that this should be incorporated into kinetic considerations. For that reason, the VT kinetic study was repeated in the presence of 2 equiv of Xantphos (approaching the plateau region; see above) and a new set of activation parameters was obtained: $\Delta H^{\neq}$ = 29.3 ± 2.8 kcal mol^{-1} and $\Delta S^{\neq}$ = 15.9 ± 8.4 e.u. These new parameters are only slightly distinguishable, within the determination errors, from the ones measured in the absence of extra Xantphos ($\Delta H^{\neq}$ = 25.9 ± 2.6 kcal mol^{-1} and $\Delta S^{\neq}$ = 6.4 ± 7.8 e.u.; see above). Nonetheless, the kinetic data (Figures S9 and S10 and Tables S1 and S3, Supporting Information) clearly indicate the trend for an increase in the effective energy barrier in the presence of Xantphos.

COMPUTATIONAL STUDIES

Density functional theory (DFT) calculations based on the dispersion-corrected functional, B97-D, have been performed in order to assess various possible mechanisms for CF_3−Ph reductive elimination from **cis-1**. As part of this study, we also modeled the dynamic behavior of **cis-1**, both to compare with the experimental NMR data and to elucidate the transition states involved in these processes.

Structure and Dynamic Behavior of cis-1. The computed structure of **cis-1** is shown in Figure 3 and compares well with the reported experimental data.[13] The metal−ligand bond lengths are reproduced to within 0.04 Å, the major discrepancy being an underestimation of the Pd−P2 bond trans to Ph (calculated, 2.43 Å, cf. experimental, 2.466 Å). Key P1−Pd−P2 and C1−Pd−C2 angles are reproduced to within 1°, and a distortion from square-planar coordination (quantified by τ, the angle between the C1−Pd−C2 and P1−Pd−P2 planes) is also reproduced, although slightly exaggerated (τ_{calc} = 34° cf. 26° experimentally).

We have characterized pathways for both the degenerate cis−cis isomerization and the cis−trans isomerization of **cis-1**. cis−cis isomerization proceeds via **TS(cis-1 - cis-1′)$_{Ph}$** with $\Delta G^{\neq}_{calc}$ = 12.8 kcal mol^{-1} in toluene, in excellent agreement with the experimental value of 13.4 kcal mol^{-1}. $\Delta G^{\neq}_{calc}$ is almost unchanged (12.9 kcal mol^{-1}) when recomputed in either THF or CH_2Cl_2, consistent with the lack of significant solvent dependence for this process. **TS(cis-1 - cis-1′)$_{Ph}$** exhibits a truncated trigonal bipyramidal structure with an axial Ph ligand and a vacant trans axial site. As the Ph ligand drops into this axial position, the CF_3 group moves to a central equatorial site (C1−Pd−P1 = 128°; C1−Pd−P2 = 127°). These movements continue after the transition state to give **cis-1′**, an equivalent structure to **cis-1**, but now with CF_3 trans to P2 and Ph trans to P1. Similar trigonal structures have been located as intermediates or transition states for intramolecular phosphine exchange in [$(R_3P)_3RhX$] complexes (R = H, Ph; X = H, Me, CF_3, Ph), and the accessibility of such processes is promoted by the high trans influence of the anionic ligands X.[23] In the present case, a second transition state, **TS(cis-1 - cis-1′)$_{CF_3}$**, was also located with now CF_3 axial and Ph equatorial. **TS(cis-1 - cis-1′)$_{CF_3}$** is only slightly higher in energy than **TS(cis-1 - cis-1′)$_{Ph}$** (G = +13.6 kcal mol^{-1}; see the Supporting Information), reflecting the similar trans influences of the Ph and CF_3 ligands. The CF_3 ligand has long been known to exhibit a very strong trans influence.[7]

The cis−trans isomerization transition state, **TS(cis-1 - trans-1)**, exhibits near C_s symmetry and is formed via simultaneous widening of both the C1−Pd−C2 and the P1−Pd−P2 angles, to 116.3° and 133.8°, respectively. During the **cis-1** to **trans-1** interconversion, the bowed structure of the Xantphos ligand backbone flips in order to accommodate the CF_3 ligand in **trans-1**, and in **TS(cis-1 - trans-1)** this moiety is nearly exactly planar. The free energy barrier to cis−trans isomerization is 21.9 kcal mol^{-1}, significantly higher than that for cis−cis isomerization and consistent with cis−trans isomerization being slow on the NMR time scale at 25 °C. **trans-1** itself is computed to be 0.9 kcal mol^{-1} less stable than **cis-1**, which is, therefore, predicted to be the dominant species at equilibrium in toluene, as is indeed observed. This difference increases to 1.2 kcal mol^{-1} in THF and 1.3 kcal mol^{-1} in CH_2Cl_2, mirroring the experimentally observed decrease in the equilibrium concentration of **trans-1** in these more polar solvents.

CF_3−Ph Reductive Elimination from cis-1. Experimental evidence suggests that **cis-1** undergoes a direct C−C reductive elimination process, and calculations based on this mechanism do reproduce the experimental behavior well. Thus, in toluene, $\Delta H^{\neq}_{calc}$ = 24.8 kcal mol^{-1} (cf. 25.9 ± 2.6 kcal mol^{-1} experimentally). Moreover, $\Delta G^{\neq}_{calc}$ = 25.0 kcal mol^{-1}, confirming a small entropic effect, and increases to 25.9 kcal mol^{-1} when recomputed in THF, consistent with the slower reaction observed experimentally in that medium. The computed reductive elimination transition state, **TS(cis-1 - 3)**, is accessed via narrowing the C1−Pd−C2 angle to 53.9° and increasing the P1−Pd−P2 angle to 110.5°. The C1−Pd−C2 plane also twists further away from square-planar coordination (τ = 46.7°); similar twisting of an originally planar reactant structure has also been computed for C(sp^2)−C(sp^3) reductive elimination from [$Pd(PH_3)_2(CH_3)(R')$] systems (R′ = Ph, vinyl).[33] In the present case, the precursor **cis-1** also exhibits significant out-of-plane distortion, suggestive of a ground-state destabilization effect. However, during conformational searches for alternative reductive elimination transition states, we located a range of structures, the most extreme of which had τ = 14.2 and 86.5° (see the Supporting Information). As both these structures remained close in energy to **TS(cis-1 - 3)**, it appears that a twisted transition-state geometry is not a necessary condition for CF_3−Ph reductive elimination in this system. In all these transition states, CF_3−Ph reductive elimination is characterized by a significant elongation of the Pd−CF_3 bond, for example, from 2.08 Å in **cis-1** to 2.38 Å in **TS(cis-1 - 3)**. In contrast, the Pd−Ph distance in **TS(cis-1 - 3)** is 2.08 Å, only 0.02 Å longer than that in **cis-1**. This has been noted before by Buchwald and co-workers,[15] who ascribed a major component of the CF_3−Ar reductive elimination barrier to Pd−CF_3 bond lengthening. The initial intermediate formed via C−C coupling from **cis-1** is **3** (G = −20.7 kcal

dx.doi.org/10.1021/om200985g | Organometallics 2012, 31, 1315−1328

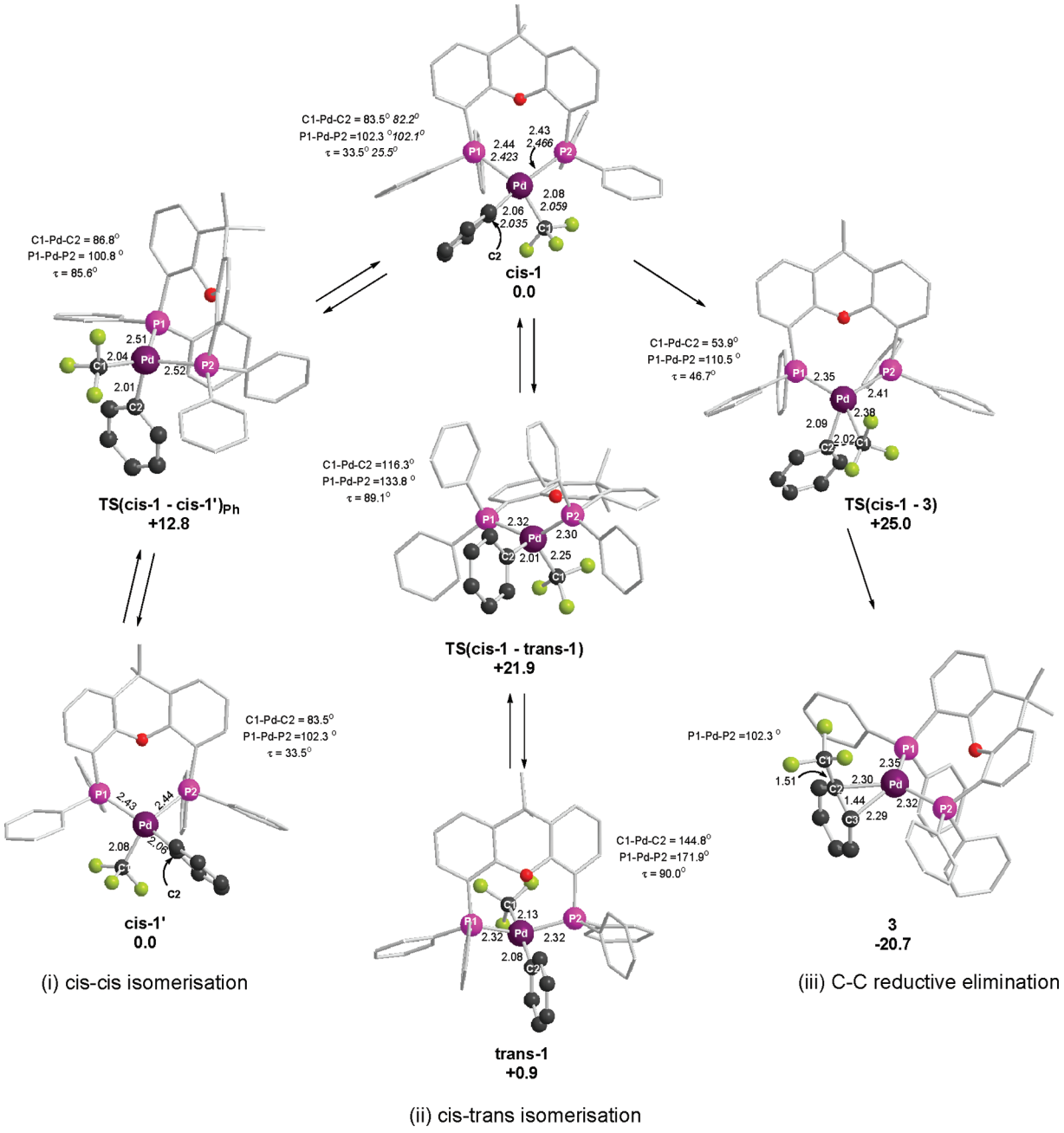

Figure 3. Computed stationary points for (i) cis−cis isomerization, (ii) cis−trans isomerization, and (iii) CF_3−Ph reductive elimination in **cis-1**. Free energies (kcal mol^{-1}) are computed in toluene, and selected distances are given in angstroms. H atoms are removed for clarity, and for **cis-1**, experimental data[11] are included in italics for comparison.

mol^{-1}), in which the $PhCF_3$ product is bound in an η^2-fashion to the {(Xantphos)Pd} moiety.

Overall, our B97-D calculations reproduce the behavior of **cis-1** very well, with cis−cis isomerization being the most accessible process ($\Delta G^{\neq}_{calc}$ = 12.8 kcal mol^{-1}), followed by cis−trans isomerization ($\Delta G^{\neq}_{calc}$ = 21.9 kcal mol^{-1}), and finally C−C reductive elimination ($\Delta G^{\neq}_{calc}$ = 25.0 kcal mol^{-1}). The barriers for cis−cis isomerization and reductive elimination are in excellent quantitative agreement with the experimental data, and observed solvation effects are also qualitatively reproduced through PCM calculations.[34]

For completeness, we have also modeled CF_3−Ph reductive elimination from [(*i*-Pr-Xantphos)Pd(Ph)(CF_3)], **2**. This species is only observed as the trans isomer, and calculations indicate that this is 10.2 kcal mol^{-1} more stable than the cis form. $\Delta G^{\neq}_{calc}$ for reductive elimination from **cis-2** is 24.0 kcal mol^{-1}, actually slightly lower than that from **cis-1**. However, the overall barrier relative to **trans-2** is 34.2 kcal mol^{-1}, and so the lack of facile CF_3−Ph reductive elimination is this case reflects the relative inaccessibility of the cis isomer. Similarly, we compute barriers in excess of 33 kcal mol^{-1} for CF_3−Ph reductive elimination from [(dppe)Pd(Ph)(CF_3)] and [(dppp)Pd(Ph)(CF_3)], consistent with the need for prolonged heating at high temperatures to observe this process experimentally in these systems.[11] Similar trends have been reported in a recent computational study of CF_3−Ph reductive elimination from [Pd(L-L)Ph(CF_3)] species that appeared during the final drafting of this work.[35]

dx.doi.org/10.1021/om200985g | *Organometallics* 2012, 31, 1315−1328

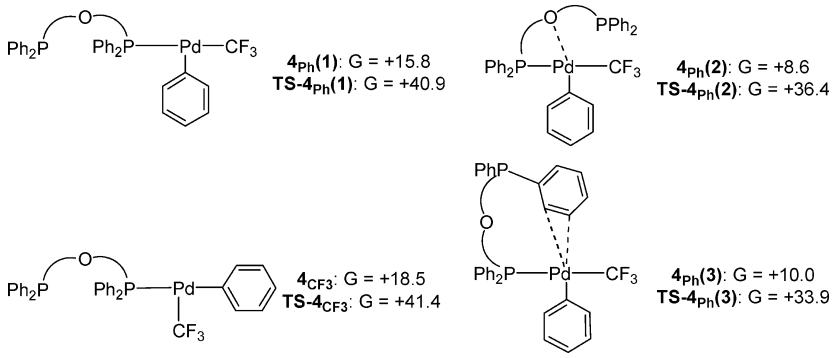

Figure 4. Schematic forms of intermediate **4**, with associated free energies computed in toluene (kcal mol^{-1}) for each species and their associated CF_3–Ph reductive elimination transition states.

CF_3–Ph Reductive Elimination from cis-1 in the Presence of Added Xantphos. Calculations have also been employed to shed light on the role of excess Xantphos in retarding the rate of reductive elimination from **cis-1**. Alternative processes may derive from an intermediate **4**, in which one phosphine arm has dissociated from **cis-1**, or from the bis-Xantphos complex [(η^1-Xantphos)$_2$Pd(Ph)(CF_3)] (**5**) that was apparently observed experimentally in low equilibrium concentration in CD_2Cl_2 (eq 3). We, therefore, need to assess the ease of phosphine dissociation from, or Xantphos addition to, **cis-1**.

The computation of phosphine binding energies in organometallic complexes, L_nM-PR_3, has received considerable attention recently as one means to test the new generation of dispersion-corrected functionals.[36] Dispersion is not well treated by standard functionals, which tend to underestimate phosphine binding energies as a result, often dramatically so, when bulky ligands are involved.[23b,37] A dispersion-corrected functional treats the intramolecular dispersion between the L_nM and PR_3 fragments within the L_nM–PR_3 complex; however, upon dissociation, the dispersion between the L_nM and PR_3 species with their environment (e.g., solvent) is either neglected or may not be well-captured by standard continuum solvation models. Thus, ligand bond dissociation energies may be severely overestimated, even when calculated with a dispersion-corrected functional. Note that these problems do not reflect the accuracy or otherwise of the DFT-D approach, but rather an incomplete modeling of the chemical system under consideration. These difficulties, and related issues associated with estimation of entropic and solvation effects, have been discussed very recently by Fey and Harvey.[38]

Against this background, we located a range of different structures for intermediate **4** with the B97-D functional, and these are shown schematically in Figure 4. The 3-coordinate T-shaped structures $\mathbf{4_{Ph}(1)}$ (G = +15.8 kcal mol^{-1}) and $\mathbf{4_{CF_3}}$ (G = +18.5 kcal mol^{-1}) are formed by phosphine arm loss (trans to Ph and CF_3, respectively), followed by the rotation of the Xantphos moiety away from the Pd center. The barriers to C–C reductive elimination from these species, ($\Delta G^{\neq}_{calc}$ = 25.1 and 22.9 kcal mol^{-1}, respectively) are similar or even slightly reduced compared to the direct process from **cis-1**. However, in both cases, the high energy of the 3-coordinate intermediate means that the overall barriers to $PhCF_3$ formation via these species are in excess of 40 kcal mol^{-1}. We also located alternative structures $\mathbf{4_{Ph}(2)}$ (G = +8.6 kcal mol^{-1}) and $\mathbf{4_{Ph}(3)}$ (G = +10.0 kcal mol^{-1}) in which the Pd–P bond trans to Ph in **cis-1** is cleaved but the orientation of the Xantphos ligand allows for stronger secondary interactions to develop, through either the oxygen or the phenyl substituents. These species are, therefore, not truly 3-coordinate and so are more accessible than $\mathbf{4_{Ph}(1)}$ or $\mathbf{4_{CF_3}}$. The lowest-energy transition state derived from these structures is $\mathbf{TS\text{-}4_{Ph}(3)}$ (Figure 5) and features significant interaction of one Xantphos Ph substituent with the metal center. However, at +33.9 kcal mol^{-1}, $\mathbf{TS\text{-}4_{Ph}(3)}$ is almost 9 kcal mol^{-1} above **TS(cis-1 - 3)** and so would not be expected to contribute significantly to the overall reductive elimination process.

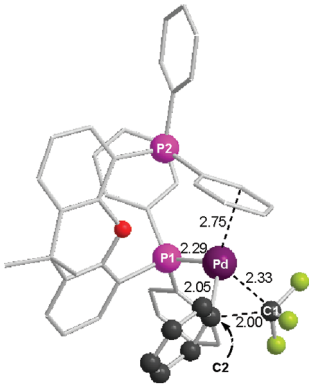

TS-4_{Ph}(3)
+33. 9

Figure 5. Computed structure of $\mathbf{TS\text{-}4_{Ph}(3)}$ with associated free energy computed in toluene in kcal mol^{-1} and selected distances given in angstroms. H atoms are removed for clarity.

Given the difficulties described above in the computation of phosphine dissociation energies, we have reoptimized the structures in Figure 4 with the BP86 functional, where no specific treatment of dispersion is included (see Figure S9 in the Supporting Information). In most cases, the relative energies decrease by between 2 and 8 kcal mol^{-1}, the only exception in fact being $\mathbf{TS\text{-}4_{Ph}(3)}$ (G = +35.4 kcal mol^{-1}). This probably reflects the retention of a significant Pd···Ph interaction in $\mathbf{TS\text{-}4_{Ph}(3)}$, which, therefore, does not involve complete ligand dissociation. This effect also means that the energies of intermediates **4** (and their associated transition states) are much less sensitive to dispersion effects than those of species **5** (see below). With the BP86 functional, the most accessible transition state is $\mathbf{TS\text{-}4_{Ph}(2)}$ (G = +30.7 kcal mol^{-1}). However, this remains 9.4 kcal mol^{-1} above **TS(cis-1 - 3)** (G =

dx.doi.org/10.1021/om200985g | *Organometallics* 2012, 31, 1315–1328

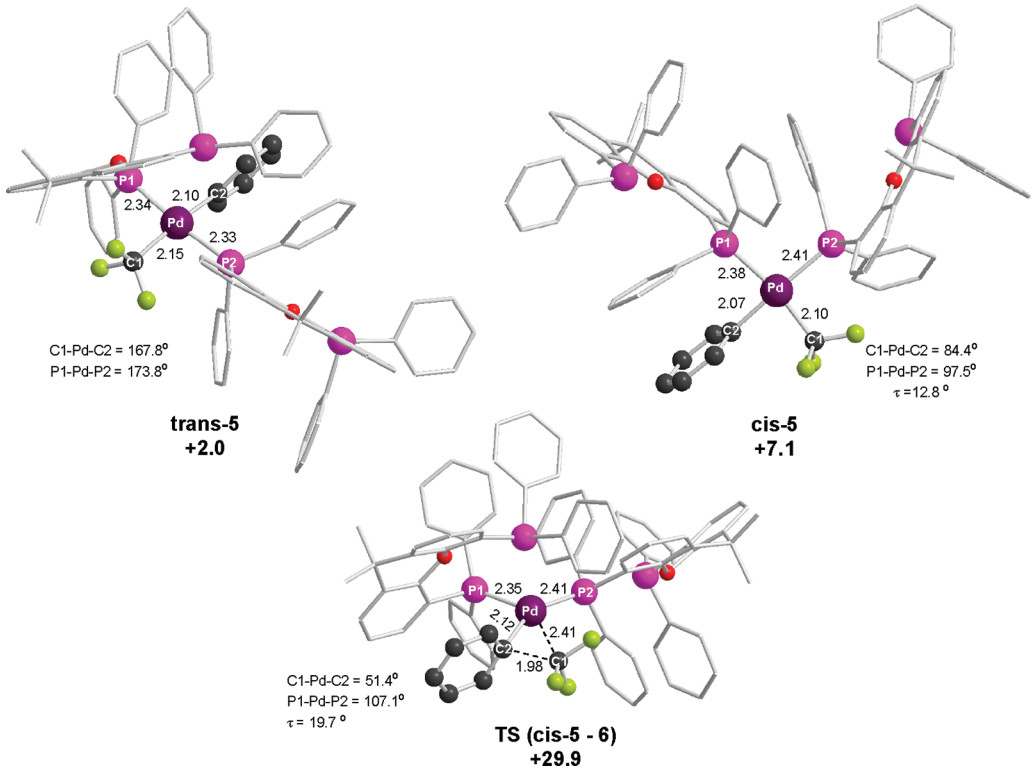

Figure 6. Computed structures of **cis-** and **trans-5** and the associated CF_3–Ph reductive elimination transition state, **TS(cis-5 - 6)**. Selected distances are given in angstroms, and H atoms are removed for clarity. Free energies in toluene are quoted relative to **cis-1** plus free Xantphos, where the free energy of **trans-5** is estimated to be +2.0 kcal mol^{-1} from its equilibrium concentration in CH_2Cl_2 at room temperature (see text for details).

+21.0 kcal mol^{-1}) when the latter is also recomputed with the BP86 functional. Thus, with the both BP86 and BP97-D functionals, the pathway via phosphine arm loss and intermediate **4** remains distinctly less accessible than the direct reductive elimination from **cis-1**.

In assessing the accessibility of $[(\eta^1\text{-Xantphos})_2Pd(Ph)(CF_3)]$, **5**, we made use of the observation that addition of excess Xantphos to **cis-1** in CH_2Cl_2 leads to an equilibrium containing a species that is formulated as *trans*-$[(\eta^1\text{-Xantphos})_2Pd(Ph)(CF_3)]$, **trans-5**, in a ca. 1:50 ratio (eq 3). This implies a free energy change of around 2 kcal mol^{-1}, and we have used this value to benchmark a range of functionals for the Xantphos addition step. We now found dramatic variation in the computed Xantphos binding free energies, consistent with the very large size of the **cis-1**/Xantphos system, with GGA and hybrid-GGA functionals severely underestimating the binding energy (BP86, BLYP, B3LYP, B3PW91: ΔG = +16 to +20 kcal mol^{-1}), whereas this was overestimated with dispersion-corrected functionals (BLYP-D, B3PW91-D,[39] B97-D, ΔG = −14 to −17 kcal mol^{-1}). With the standard B97-D (toluene) approach a value of −15.1 kcal mol^{-1} is obtained, where the solvent correction amounts to only 1.5 kcal mol^{-1}. Given these difficulties, we decided to estimate the free energy of **trans-5** based on the equilibrium concentration of this species as per eq 3; that is, **trans-5** should lie approximately 2 kcal mol^{-1} above **cis-1** plus free Xantphos. As the subsequent reductive elimination from *cis*-$[(\eta^1\text{-Xantphos})_2Pd(Ph)(CF_3)]$ then involves no change in molecularity, the barrier to this process should be less sensitive to the methodology employed and, therefore, bear comparison to the earlier results on **cis-1** and intermediate **4**.

The computed structures of the lowest-energy conformation of both **cis-5** and **trans-5**, as well as the associated CF_3–Ph reductive elimination transition state, **TS(cis-5 - 6)**, are shown in Figure 6. Both **trans-5** and **cis-5** exhibit regular square-planar coordination geometries, and **cis-5** is 5.1 kcal mol^{-1} less stable than **trans-5**, reflecting the usual preference for the trans isomer in $[(PR_3)_2Pd(X)(Ph)]$ species. The major change in accessing **TS(cis-5 - 6)** is again the lengthening of the Pd–CF_3 distance, in this case by ca. 0.3 Å. Much less distortion of the CF_3–Pd–Ph unit is seen in both **cis-5** (τ = 12.8°) and **TS(cis-5 - 6)** (τ = 19.7°), suggesting that the more flexible bis-Xantphos coordination mode imposes less steric pressure on the system than the chelate ligand in **cis-1** and **TS(cis-1 - 3)**. Despite this, the barrier to reductive elimination relative to **cis-5** is only 22.8 kcal mol^{-1}, the lowest value for this step computed in this study. Relative to **trans-5**, this equates to a barrier of 27.9 kcal mol^{-1}, rising to 29.9 kcal mol^{-1} relative to **cis-1** plus free Xantphos. CF_3–Ph reductive elimination through bis-Xantphos **cis-5** is, therefore, computed to be more accessible than through the phosphine-dissociated intermediate **4**, and the calculations suggest that **cis-1** and **cis-5** may both contribute to the reductive elimination process.

DISCUSSION

The above-described experimental and computational studies suggest that the CF_3–Ph reductive elimination from **1** occurs from its cis isomer and does not require Pd–P bond dissociation. However, a key factor strongly influencing the interpretation of the first-order kinetic data obtained experimentally for the formation of $PhCF_3$ from **1** is the unexpected effect of the extra Xantphos ligand on the measured reaction rate. While being slower in the presence of an extra

dx.doi.org/10.1021/om200985g | *Organometallics* 2012, 31, 1315–1328

Scheme 4

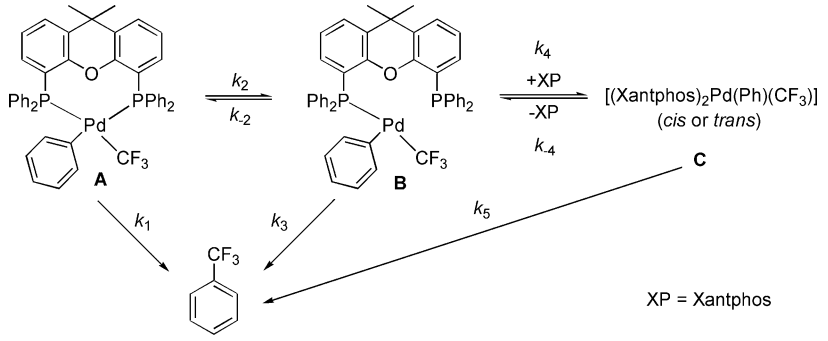

ligand, the reaction still occurs even in the presence of a 20-fold excess of Xantphos. As mentioned above, the extra Xantphos effect could, a priori, be rationalized in terms of specific or nonspecific interactions between molecules of **1** and Xantphos, which reduce the ground-state energy of **1** and act rapidly in a prekinetic step of the process. Such intermolecular interactions would lead to a larger inertia moment of short-living **1**·Xantphos, which, in turn, should reduce the correlation times of molecular reorientations. The reduced correlation times would then be well detected as a considerable decrease in T_1 times measured for Xantphos in the presence of **1**.[29] However, no such effect was observed as the ^{31}P T_1 time of Xantphos did not change in the presence of **1** (Table 2). Therefore, the extra Xantphos effect should be included in the kinetic considerations.

Kinetic Scheme 4 displays possible mechanistic pathways to $PhCF_3$ from **1**. To follow the tradition of using letter characters for reactive species in kinetic equations, we depict, in Scheme 4, **cis-1** as **A**, its open form **4** as **B**, **5** (a product of addition of Xantphos to **4**) as **C**, and Xantphos as XP. Cis−trans isomerization of **1** is not included in the kinetic scheme because this process is faster than the $PhCF_3$ formation. As shown above, the equilibrium between **cis-1** and **trans-1** establishes within the time of dissolution even at room temperature, and calculations confirm the lower barrier associated with cis−trans isomerization compared with reductive elimination. Although only **trans-5** could be observed by ^{19}F and ^{31}P NMR (eq 3), **cis-5** is more likely to undergo C−C reductive elimination. Despite the fact that **cis-5** is computed to be 5.1 kcal mol^{-1} less stable than **trans-5** (see above), both isomers should be easily accessible from **cis-1** via **4**. Two conclusions follow from Scheme 4. First, if **B** is not involved (k_2 = 0), then the CF_3−Ph reductive elimination proceeds directly from **A** and should not be influenced by extra Xantphos. Therefore, the Xantphos effect suggests that **B** should be involved as a kinetically significant species. Second, if the final product ($PhCF_3$) is formed only from **B**, Xantphos in sufficiently large excess should suppress the reaction altogether. As this is inconsistent with the experimental results, the formation of $PhCF_3$ in the absence of Xantphos occurs from **A** and, possibly, **B**. In the presence of Xantphos, **C** is formed, which may also decompose to $PhCF_3$ (Scheme 4). Two general cases can be considered.

Case 1. All three species, **A**, **B**, and **C**, produce $PhCF_3$ (Scheme 4). The rate law for this case (eq 4) is derived on the basis of formal kinetics, with intermediates **B** and **C** being present in quasi-stationary concentrations.

$$\frac{dA}{dt} = -[A]\,\frac{(k_{-4}+k_5)(k_1k_{-2}+k_1k_3+k_2k_3)+k_4k_5(k_1+k_2)[XP]}{(k_{-4}+k_5)(k_{-2}+k_3)+k_4k_5[XP]} \quad (4)$$

As eq 4 includes [XP], k_{obs} may depend on the Xantphos concentration in the system. However, if $k_5 = 0$ (**C** exists in *fast* equilibrium with **B** but does not decompose to $PhCF_3$), or if $k_4 = 0$ (no conversion of **B** to **C**), the reaction should be independent of [XP]. In other words, only the formation of **C** and its transformation to $PhCF_3$ can account for the extra Xantphos effect within this model. Figure 7 displays the fitting

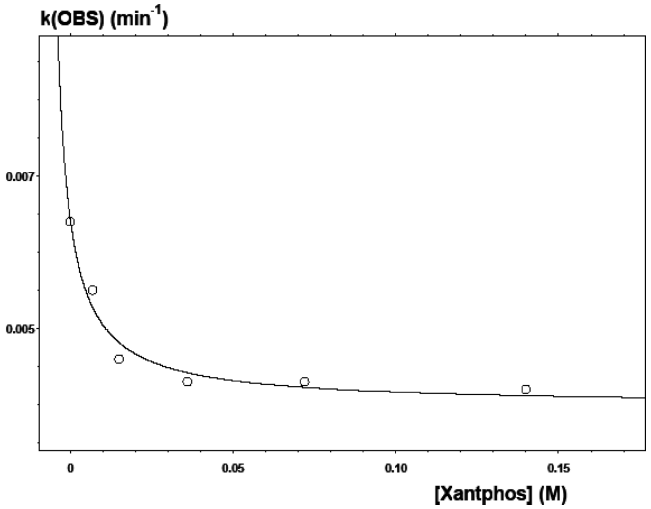

Figure 7. Dependence of k_{obs} on Xantphos concentration at 70 °C, fitted to $y = (ab + cdx)/(af + dx)$, where $y = k_{obs}$, $c = (k_1 + k_2)$, and $x =$ [XP].

of the experimental rate constants described above to the equation $y = (ab + cdx)/(af + dx)$, where $y = k_{obs}$, $c = (k_1 + k_2)$, and x = [XP], as performed with a standard program package. Because of the large number of unknowns, these fitting procedures are obviously not single-valued. The $y(x)$ function, however, is critical to the magnitude of constant $c = k_1 + k_2$, i.e. the experimentally observed dependence of k_{obs} on [XP] can be reproduced only for $k_1 + k_2 = 0.004$ min^{-1} or for $k_2 = 0.004$ min^{-1} if $k_1 = 0$ ($PhCF_3$ formation occurs only from **B** and/or **C**). It is noteworthy that the k_{obs} determination error of ca. 15% (see above) is large for the magnitude of the Xantphos effect observed, that is, the decrease of k_{obs} by only ca. 50% when going from [XP] = 0 to [XP] = 2−20 × [**1**].[40] Being reproducible, however, the effect ought to be discussed using the available results, yet the experimental errors should be kept

dx.doi.org/10.1021/om200985g | *Organometallics* 2012, 31, 1315−1328

in mind and care exercised when drawing conclusions from the data shown in Figure 7.

If the equilibrium between **A** and **B** (Scheme 4) was fast on the NMR time scale, it would contribute to the observed temperature dependence of the ^{19}F and ^{31}P NMR spectra of **cis-1** (**A**). However, the obtained value of $c = k_1 + k_2 = 0.004$ min^{-1} shows that the equilibrium between **A** and **B** is slow, in accord with the VT NMR analysis of the degenerate isomerization of **cis-1** (13.4 kcal mol^{-1} in toluene; see Table 1; $\Delta G^{\neq}_{calc}$ = 12.8 kcal mol^{-1}) and in agreement with the computed free energy cost (+15.9 kcal mol^{-1}) for full dissociation of one of the Pd−P bonds in **1** (see above).

This kinetic model suggests that, in the absence of extra Xantphos ([XP] = 0), CF_3−Ph reductive elimination can proceed directly from **A** and/or from its open form **B**. In the presence of extra Xantphos, however, the formation of $PhCF_3$ from **B** (k_3 in eq 4) is, to some extent, suppressed, yet an additional, slower pathway to $PhCF_3$ via **C** becomes operational.

Case 2. Only **A** and **C** give rise to $PhCF_3$, whereas **B** forms in the reaction but does not undergo CF_3−Ph reductive elimination. In this case, $k_3 = 0$ and, therefore, eq 4 transforms to eq 5.[41] Like in Case 1, in this case the fitting (Figure 7) shows that the corresponding $y(x)$ function is critical to the magnitude of $c = (k_1 + k_2) = 0.004$ min^{-1}.

$$\frac{dA}{dt} = -[A]\,\frac{k_1k_{-2}(k_{-4} + k_5) + k_4k_5(k_1 + k_2)[XP]}{k_{-2}(k_{-4} + k_5) + k_4k_5[XP]} \qquad (5)$$

Although Cases 1 and 2 are kinetically indistinguishable,[42] our computational results suggest that Case 1 is improbable because of the prohibitively high (>40 kcal mol^{-1}) barrier to reductive elimination from **B**. Case 2, however, is consistent with both experimental and computational data pointing to realistic free energy values for $PhCF_3$ reductive elimination from **A** (25.0 kcal mol^{-1}) and from **cis-C** (29.9 kcal mol^{-1}). These numbers are in good agreement with the experimentally determined activation parameters $\Delta H^{\neq}$ = 25.9 ± 2.6 kcal mol^{-1} and $\Delta S^{\neq}$ = 6.4 ± 7.8 e.u. (in the absence of extra Xantphos), and $\Delta H^{\neq}$ = 29.3 ± 2.8 kcal mol^{-1} and $\Delta S^{\neq}$ = 15.9 ± 8.4 e.u. (in the presence of 2 equiv of Xantphos).

As mentioned above, three events could, in principle, account for the Xantphos effect, i.e. the CF_3−Ph bond formation from **1** is (i) governed by two mechanistic pathways with similar barriers, of which one is altered by an extra ligand; (ii) catalyzed by some species that are sequestered by Xantphos; and (iii) influenced by changes in properties of the medium in the vicinity of **1** in the presence of Xantphos and/or by specific interactions between **1** and Xantphos. While we have demonstrated plausibility of item (i) and ruled out item (iii) by the T_1 studies, a comment is due on item (ii) that is catalysis of reaction 1 by a small quantity of some species that may be present in the sample of **1** and/or produced during the reaction, and that are deactivated by extra Xantphos. Apparently this scenario can be ruled out, too. The sample of **1** used in this work was spectroscopically pure and, therefore, could only contain impurities in the amount of <1%. Therefore, the molar ratio of Xantphos used in the studies (1−20 equiv to **1**) to this impurity would be in the range of 100−2000, i.e. the scavenging of the catalytically active species would be pseudo-zero-order in Xantphos in all of the runs and no dependence of k_{obs} for the formation of $PhCF_3$ from **1** on [Xantphos] would be observed.

It is worth reemphasizing that two major assumptions have been made in this work regarding **C**. First, the ^{19}F and ^{31}P NMR signals observed from the minor species emerging on addition of excess Xantphos to **1** are fully consistent with the formulation of *trans*-[(η^1-Xantphos)$_2$Pd(Ph)(CF_3)] (**trans-C**), as shown in eq 3. However, no unambiguous evidence for this formulation (e.g., an X-ray structure) could be obtained because of the low concentration of this species and its lability toward ligand loss leading to **1**. Also, as described above, the limited solubility of **1** in toluene at room temperature precluded determination of K_{eq} for reaction 3 in this solvent that was used in the kinetic studies. Therefore, the K_{eq} was determined in CH_2Cl_2, a solvent that would likely affect the rate of decomposition of **1** and that could not be used in the kinetic study because of its low boiling point of 40 °C. Second, the computed figure for the overall barrier to CF_3−Ph reductive elimination from **cis-C** (29.9 kcal mol^{-1}) heavily relies on the first assumption and suffers from the incomplete modeling of the ligand addition process, in particular, solute−solvent dispersive interactions, as discussed in detail above.

Importantly, however, these assumption-based studies have produced a more reliable computed number of only 22.8 kcal mol^{-1} for the barrier to CF_3−Ph reductive elimination from **cis-C**. We believe that this result may be viewed as a guideline for the development of other ligands for CF_3−Ar bond formation at Pd(II). Apparently, a wide bite angle phosphine is not a critical requirement for facile CF_3−Ph reductive elimination from Pd(II), and it is conceivable that bulky enough ligands that nonetheless can adopt cis configuration on Pd may appear suitable for the desired transformation.

A comment is also due on the suitability of Xantphos for Pd-catalyzed trifluoromethylation of aromatic electrophiles, such as haloarenes (Scheme 5). We think that this catalytic trans-

Scheme 5

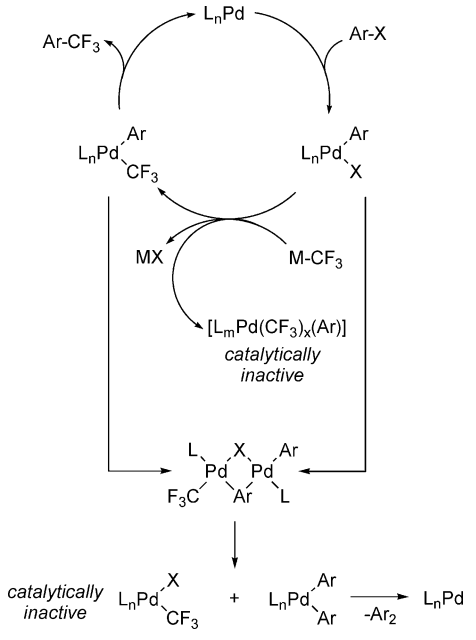

formation is unlikely to be developed with Xantphos, despite the facile CF_3−Ph reductive elimination from **1**. One of the problems emerges at the nucleophilic trifluoromethylation of the Pd−X bond in [(Xantphos)Pd(Ar)(X)] that is formed in the Ar-X oxidative addition step. The "CF_3^-" equivalents

dx.doi.org/10.1021/om200985g | *Organometallics* 2012, 31, 1315−1328

conventionally used for the Pd−CF_3 bond formation, e.g., CF_3SiMe_3/F^-, easily and irreversibly displace not only halides on the metal but also the stabilizing tertiary phosphines[11,13,43] to give catalytically inactive poly(trifluoromethyl) complexes (shown as $[L_mPd(CF_3)_x(Ar)]$ in Scheme 5). This transformation is avoided only for Pd complexes of tightly binding chelating ligands, such as dppe, dppp, and tmeda,[11] but not Xantphos.[13] A less widely recognized, yet perhaps more general, problem is the enhanced ability of trifluoromethyl Pd aryls to undergo transmetalation with other aryl Pd complexes, including [(Xantphos)Pd(Ar)(X)], a key intermediate that is formed in the oxidative addition step. As a result, [(Xantphos)-Pd(Ar)(X)] and [(Xantphos)Pd(CF_3)(Ar)] react to give catalytically inactive [(Xantphos)Pd(CF_3)(X)] and [(Xantphos)Pd$(Ar)_2$], the latter quickly undergoing Ar−Ar reductive elimination (Scheme 5). Like numerous other transmetalation reactions, this documented[11,13] catalyst deactivation pathway should be facilitated by "nucleophilic aid", that is, coordination of the halide ligand X to the Pd atom bearing the CF_3 ligand. As the CF_3 ligand stabilizes[7] orbitals on the metal, LUMO included, this halide ligand coordination (bridging) should be favored, contributing to the transmetalation process. We propose that this might be a reason for aryl chlorides being much better substrates than aryl bromides for Buchwald's Pd-catalyzed trifluoromethylation[15] because LPd(Ar)X transmetalates LPd(Ar)CF_3 more easily for X = Br that is more electron-rich than Cl. Ways to minimize the transmetalation leading to catalyst deactivation should be to use ArX substrates that are derivatives of less nucleophilic X^- and run the process at lower concentrations of Pd to slow down transmetalation that is a bimolecular reaction.

CONCLUSIONS

Two trifluoromethyl Pd(II) phenyl complexes, [(Xantphos)-Pd(Ph)(CF_3)] (**1**) and [(*i*-Pr-Xantphos)Pd(Ph)(CF_3)] (**2**), have been studied by experimental and computational methods. Complex **1** is exclusively cis in the solid state and predominantly cis in solution, undergoing degenerate cis−cis isomerization ($\Delta G^{\neq}_{exp}$ = 13.4 kcal mol^{-1}; $\Delta G^{\neq}_{calc}$ = 12.8 kcal mol^{-1} in toluene) that is much less energy demanding than its cis−trans isomerization ($\Delta G^{\neq}_{calc}$ = 21.9 kcal mol^{-1}). In accord with the experimental data, **cis-1** is computed to be ca. 1 kcal mol^{-1} more stable than **trans-1**. In contrast, **2** is only observed as the trans isomer in both solution and the solid state (NMR, X-ray), also in full accord with the much higher free energy (+10.2 kcal mol^{-1}) for the cis isomer in this case.

As previously communicated,[13] **1** undergoes remarkably facile CF_3−Ph reductive elimination from Pd(II) under mild conditions to give $PhCF_3$ in high yield. Kinetic and computational studies of $PhCF_3$ formation from **1** indicated that the reductive elimination does not require P−Pd bond dissociation but rather occurs directly from the cis isomer. The experimentally determined activation parameters ($\Delta H^{\neq}$ = 25.9 ± 2.6 kcal mol^{-1}; $\Delta S^{\neq}$ = 6.4 ± 7.8 e.u.) are in excellent agreement with the computed data ($\Delta H^{\neq}_{calc}$ = 24.8 kcal mol^{-1}; $\Delta G^{\neq}_{calc}$ = 25.0 kcal mol^{-1}). Interestingly, $\Delta G^{\neq}_{calc}$ for CF_3−Ph reductive elimination from **cis-2** is 24.0 kcal mol^{-1}, slightly lower than that from **cis-1**. Nonetheless, the overall barrier relative to **trans-2** is much higher ($\Delta G^{\neq}_{calc}$ = 34.2 kcal mol^{-1}) as it includes the high energy cost of 10.2 kcal mol^{-1} to isomerize **trans-2** to **cis-2**. This is consistent with the higher thermal stability of **2** that decomposes to $PhCF_3$ only at 100 °C, and even then only in a sluggish and less-selective manner.

An interesting effect of extra Xantphos has been observed on the rate of decomposition of **1** at 70 °C. In the presence of 1 and 2 equiv of Xantphos, a steady slight decrease in k_{obs} is detected, which then plateaus at Xantphos:**1** = 5, 10, and 20, the overall drop in reaction rate being only ca. 50%. A series of T_1 measurements indicated that this minor effect is not caused by changes in either the properties of the medium or weak specific molecular interactions between **1** and Xantphos. A kinetic scheme has been proposed that accounts for the Xantphos effect and involves the formation of [(η^1-Xantphos)$_2$Pd(Ph)(CF_3)] (**5**) in small quantities from **1** and the excess ligand. A computational study prompted by the kinetic scheme gave $\Delta G^{\neq}_{calc}$ = 22.8 kcal mol^{-1} for CF_3−Ph reductive elimination from **cis-5**, the lowest barrier for this step computed in the present work. The energy of **cis-5** relative to **cis-1** and free Xantphos could not be accurately assessed because of the difficulty in capturing all environmental effects with the current chemical model system. Importantly, however, the low barrier to CF_3−Ph bond formation from **cis-5** implies that a wide bite angle diphosphine is not a critical requirement for facile CF_3−Ph bond formation at Pd(II) and that bulky enough ligands able to adopt a cis configuration on Pd may appear suitable for the desired transformation.

EXPERIMENTAL SECTION

All chemicals were purchased from Aldrich, Alfa Aesar, and Apollo Scientific. All manipulations were performed under argon in a glovebox. Benzene, toluene, and THF were distilled from Na/$OCPh_2$ and stored over 4 Å molecular sieves in a glovebox. *i*-Pr-Xantphos[44] and [$(Ph_3P)_2$Pd(Ph)(Br)][45] were synthesized by the literature procedures. Routine NMR spectra were recorded on a Bruker Avance 400 Ultrashield spectrometer equipped with a BBFO plus SmartProbe. A Bruker Avance 500 Ultrashield NMR instrument equipped with a BBI probe was used for VT NMR and kinetic studies. ^{31}P T_1 time measurements were performed using a Bruker Avance III 500 Ultrashield NMR spectrometer equipped with a QNP CryoProbe. The standard inversion−recovery method was applied to collect the data that were treated to calculate T_1. All NMR data were processed with the Topspin 2.1 Bruker software. A Bruker-Nonius diffractometer equipped with an Apex II 4K CCD area detector was used for single-crystal diffraction studies. An Agilent Technologies 7890A chromatograph equipped with a 5975C MSD unit was used for GC-MS analysis. Elemental analyses were performed by the Microanalysis Center at the Complutense University of Madrid.

Preparation of [(Xantphos)Pd(Ph)(CF_3)] (1). This complex was prepared using our previously developed[13] procedure, except [(Xantphos)Pd(Ph)(F)] was generated from [(Xantphos)Pd(Ph)(I)] and AgF in the presence of 5 mol % PhI and 5 mol % Xantphos (see above).

Preparation of [(*i*-Pr-Xantphos)Pd(Ph)(CF_3)] (2). A mixture of *i*-Pr-Xantphos (0.20 g, 0.45 mmol) and [$(Ph_3P)_2$Pd(Ph)(Br)] (0.27 g, 0.34 mmol) in THF (5 mL) was gently warmed to 50 °C at stirring until all solids had dissolved to produce a yellow solution. After 36 h at room temperature, the equilibrated mixture contained [(*i*-Pr-Xantphos)Pd(Ph)(Br)] and [$(Ph_3P)_2$Pd(Ph)(Br)] in a 92:8 molar ratio (^{31}P NMR). This solution was vigorously stirred with CsF (0.10 g, 0.66 mmol) and CF_3SiMe_3 (0.10 mL, 0.68 mmol) for 4.5 h. Extra CF_3SiMe_3 (0.05 mL, 0.34 mmol) was then added, and after stirring for 2 more hours, full conversion was observed by ^{31}P NMR. The solution was evaporated in air and the residue extracted with CH_2Cl_2 (5 mL). The extract was filtered, evaporated to ca. 0.5 mL, and treated with MeOH (15 mL in portions). After 1 h, the pale tan, well-shaped crystals were separated, washed with MeOH, and dried under vacuum. The yield of **2** was 0.13 g (55%). X-ray quality crystals were grown from benzene−MeOH. Calcd for $C_{34}H_{45}F_3OP_2Pd$: C, 58.75; H, 6.52. Found: C, 58.70; H, 6.45. ^{1}H NMR (C_6D_6, 25 °C), δ: 0.3 (q, J = 7.1 Hz, 6H, CH_3CH), 0.85 (q, J = 6.3 Hz, 6H, CH_3CH), 1.3 (s, 3H, arom-

dx.doi.org/10.1021/om200985g | *Organometallics* 2012, 31, 1315−1328

CH_3), 1.4 (q, J = 7.6 Hz, 6H, CH_3CH), 1.5 (m, 6H, CH_3CH), 1.65 (s, 3H, arom-CH_3), 2.3 (m, 2H, $CHCH_3$), 3.15 (m, 2H, $CHCH_3$), 5.6 (d, J = 7.5 Hz, 1H, σ-C_6H_5), 6.35 (t, J = 7.5 Hz, 1H, σ-C_6H_5), 6.65 (t, J = 7.2 Hz, 1H, σ-C_6H_5), 6.85 (m, 2H, arom H), 6.95 (t, J = 7.4 Hz, 1H, σ-C_6H_5), 7.05 (t, J = 7.7 Hz, 2H, arom H), 7.35 (dd, J = 7.7 and 1.5 Hz, 2H, arom H), 8.4 (d, J = 7.5 Hz, 1H, σ-C_6H_5). ^{19}F NMR (C_6D_6, 25 °C), δ: −13.1 (t, J_{F-P} = 13.8 Hz). ^{31}P NMR (C_6D_6, 25 °C), δ: 20.0 (q, J_{F-P} = 13.8 Hz).

Determination of K_{eq} for the Reaction of 1 with Xantphos. Addition of recrystallized Xantphos (140 mg, 0.24 mmol) to a solution of **1** (10 mg, 1.2×10^{-2} mmol) in CD_2Cl_2 (0.6 mL) in a 5 mm NMR tube resulted in the appearance of new signals in the NMR spectra. In the ^{19}F NMR spectrum, a new triplet emerged at −19.7 ppm (J_{P-F} = 24 Hz). In the ^{31}P NMR spectrum, a quartet at 16.1 ppm with the same coupling constant (J_{P-F} = 24 Hz) and a singlet of the same integral intensity at −19.5 ppm were observed. These data are consistent with the structure of *trans*-[(η^1-Xantphos)$_2$Pd(Ph)(CF_3)]. Integration of the new signals against those from **1** allowed for the determination of the molar ratio of *trans*-[(η^1-Xantphos)$_2$Pd(Ph)-(CF_3)] to **1** at ca. 1:50. On the basis of these data, K_{eq} between **1** + Xantphos and *trans*-[(η^1-Xantphos)$_2$Pd(Ph)(CF_3)] in CD_2Cl_2 at 25 °C was estimated at ca. 5×10^{-2} L mol^{-1}.

Kinetic Measurements. In a glovebox, a 5 mm NMR tube was charged with **1** (4 mg), Xantphos (in certain experiments), and toluene (0.7 mL). The sample was quickly sonicated at room temperature to facilitate dissolution of **1** and placed in the preheated probe of an NMR spectrometer. The reactions were followed by ^{19}F NMR spectroscopy (NS = 64 − 256; D1 = 5 s; SW = 200 ppm) and k_{obs} derived from plots of integral intensities of the signals from $PhCF_3$ and **1** versus time. The spectra were automatically measured every 15 min for the runs at 80 and 70 °C, and every 30 min and 1 h for the runs at 60 and 50 °C, respectively. The concentration of **1** used (6.9 mM) was close to the solubility of the complex in toluene at room temperature and to the lower limit for accurate rate measurements by integration of the signals from **1** and from the product, $PhCF_3$. Higher concentrations of **1** could not be used because of its limited solubility in toluene. Exponential fittings were performed using the SPECFIT[46] software. All traces were fitted to a single exponential model. No significant difference in the calculated constants was observed between the [(Xantphos)Pd(Ph)(CF_3)] and $PhCF_3$ plots. In all cases, the final values reported in the Supporting Information correspond to average of all calculated constants for experiments under the same conditions.

Computational Details. Calculations were run with Gaussian 09[47] with geometry optimizations using the B97-D dispersion corrected functional.[48] Pd and P centers were described with the Stuttgart RECPs and associated basis sets,[49] with added d-orbital polarization on P (ζ = 0.387).[50] 6-31G** basis sets were used for all other atoms.[51] All stationary points were fully characterized via analytical frequency calculations as either minima (all positive eigenvalues) or transition states (one negative eigenvalue), and IRC calculations and subsequent geometry optimizations were used to confirm the minima linked by each transition state. Extensive functional tests were carried out on the barrier to reductive elimination from **cis-1**, and the inclusion of dispersion effects was found to increase the barrier for this process and so produce better agreement with experiment. See the Supporting Information for details. All stationary points were subject to extensive conformational searching using our recently published protocol.[52] Free energies are computed at 298.15 K and 1 atm pressure, and solvation effects are included through the PCM approach, using UFF atomic radii.

■ ASSOCIATED CONTENT

Supporting Information

VT NMR spectra, rate constants, Eyring plots, alternative kinetic models, and details of computational (PDF, including full ref 47) and crystallographic studies (CIF). This material is available free of charge via the Internet at http://pubs.acs.org.

■ AUTHOR INFORMATION

Corresponding Author

*E-mail: vgrushin@iciq.es (V.V.G.), s.a.macgregor@hw.ac.uk (S.A.M.), bakhmoutov@mail.chem.tamu.edu (V.I.B.).

■ ACKNOWLEDGMENTS

We thank Prof. José Ramón Galán-Mascarós for a discussion. The ICIQ Foundation and Consolider Ingenio 2010 (Grant CSD2006-0003) are thankfully acknowledged for support, as are the EPSRC and Heriot-Watt University for a doctoral training award to J.A.P.

■ REFERENCES

(1) For selected monographs, see: (a) Clark, J. H.; Wails, D.; Bastock, T. W. *Aromatic Fluorination*; CRC Press: Boca Raton, FL, 1996. (b) Kirsch, P. *Modern Fluoroorganic Chemistry*; Wiley-VCH: Weinheim, Germany, 2004. (c) Uneyama, K. *Organofluorine Chemistry*; Blackwell: Oxford, U. K., 2006. (d) Ojima, I. *Fluorine in Medicinal Chemistry and Chemical Biology*; Wiley-Blackwell: Chichester, U. K., 2009.

(2) Burton, D. J.; Yang, Z. Y. *Tetrahedron* **1992**, *48*, 189.

(3) McClinton, M. A.; McClinton, D. A. *Tetrahedron* **1992**, *48*, 6555.

(4) Burton, D. J.; Lu, L. *Top. Curr. Chem.* **1997**, *193*, 45.

(5) Schlosser, M. *Angew. Chem., Int. Ed.* **2006**, *45*, 5432.

(6) Roy, S.; Gregg, B. T.; Gribble, G. W.; Le, V.-D.; Roy, S. *Tetrahedron* **2011**, *67*, 2161.

(7) Tomashenko, O. A.; Grushin, V. V. *Chem. Rev.* **2011**, *111*, 4475.

(8) Filler, R. *Adv. Fluorine Chem.* **1970**, *6*, 1.

(9) (a) Inoue, M.; Araki, K. Jpn. Patent JP 2009-234921, 2009. (b) Oishi, M.; Kondo, H.; Amii, H. *Chem. Commun.* **2009**, 1909. (c) Knauber, T.; Arikan, F.; Röschenthaler, G.-V.; Gooßen, L. J. *Chem.—Eur. J.* **2011**, *17*, 2689. (d) Popov, I.; Lindeman, S.; Daugulis, O. *J. Am. Chem. Soc.* **2011**, *133*, 9286. (e) Weng, Z.; Lee, R.; Jia, W.; Yuan, Y.; Wang, W.; Feng, X.; Huang, K.-W. *Organometallics* **2011**, *30*, 3229. (f) Li, Y.; Chen, T.; Wang, H.; Zhang, R.; Jin, K.; Wang, X.; Duan, C. *Synlett* **2011**, 1713.

(10) Culkin, D. A.; Hartwig, J. F. *Organometallics* **2004**, *23*, 3398.

(11) Grushin, V. V.; Marshall, W. J. *J. Am. Chem. Soc.* **2006**, *128*, 4632.

(12) (a) Ozawa, F.; Kurihara, K.; Fujimori, M.; Hidaka, T.; Toyoshima, T.; Yamamoto, A. *Organometallics* **1989**, *8*, 180. (b) Brown, J. M.; Guiry, P. J. *Inorg. Chim. Acta* **1994**, *220*, 249.

(13) Grushin, V. V.; Marshall, W. J. *J. Am. Chem. Soc.* **2006**, *128*, 12644.

(14) Grushin, V. V. *Acc. Chem. Res.* **2010**, *43*, 160.

(15) Cho, E. J.; Senecal, T. D.; Kinzel, T.; Zhang, Y.; Watson, D. A.; Buchwald, S. L. *Science* **2010**, *328*, 1679.

(16) CF_3−Ar bond formation at Pd(IV) has been recently reported: (a) Ball, N. D.; Kampf, J. W.; Sanford, M. S. *J. Am. Chem. Soc.* **2010**, *132*, 2878. (b) Ye, Y.; Ball, N. D.; Kampf, J. W.; Sanford, M. S. *J. Am. Chem. Soc.* **2010**, *132*, 14682. (c) Ball, N. D.; Gary, J. B.; Ye, Y.; Sanford, M. S. *J. Am. Chem. Soc.* **2011**, *133*, 7577.

(17) (a) Fraser, S. L.; Antipin, M. Yu.; Khroustalyov, V. N.; Grushin, V. V. *J. Am. Chem. Soc.* **1997**, *119*, 4769. (b) Pilon, M. C.; Grushin, V. V. *Organometallics* **1998**, *17*, 1774.

(18) Complete removal ofwater from AgF originating from aqueous solutions is virtually impossible: Horn, E.; Snow, M. R. *Aust. J. Chem.* **1980**, *33*, 2369.

(19) Instead, the reaction produced a stable zerovalent Pd complex that is formulated as [(*i*-Pr-Xantphos)$_2$Pd$_2$(dba)] on the basis of the ^{1}H NMR data. Numerous attempts to obtain X-ray quality crystals of this complex failed, mostly because the compound crystallizes as extremely thin, fiber-like needles that are not suitable for single-crystal X-ray analysis. Heating of the complex in the presence of PhBr did not produce selectively [(*i*-Pr-Xantphos)Pd(Ph)(Br)] for the synthesis of **2**, but rather a mixture of complexes, including a product of dba migratory insertion into a Pd−Ph bond (^{1}H NMR).

(20) ^{1}H NMR for [(*i*-Pr-Xantphos)Pd(Ph)(Br)] (CD_2Cl_2, 25 °C), δ: 1.05 (m, 12H, *i*-Pr-CH_3), 1.3 (m, 12H, *i*-Pr-CH_3), 1.8 (s, 6H, xanthene-CH_3), 2.6 (m, 4H, *i*-Pr-CH), 7.1 (t, 1H, 4-PdPh), 7.2 (t, 2H, 3-PdPh), 7.4 (dm, 2H, 2-PdPh), 7.5 (tt, J = 7.5 and 0.7 Hz, 2H, xanthene-CH), 7.55 (m, 2H, xanthene-CH), 7.85 (dd, J = 7.5 and 2.0 Hz, 2H, xanthene-CH). The structure of [(*i*-Pr-Xantphos)Pd(Ph)(Br)] in solution strongly depends on the polarity of the medium. CD_2Cl_2 solutions of this complex are colorless, displaying a singlet in the ^{31}P NMR spectra at 34.4 ppm, whereas in benzene and THF, the complex is bright yellow, resonating at 15.2 and 14.9 ppm, respectively. The significant difference in the ^{31}P NMR chemical shifts as well as in color indicates that, in less-polar benzene and THF, the complex exists as a neutral species [(*i*-Pr-Xantphos)Pd(Ph)(Br)], whereas in more polar CD_2Cl_2, it is ionic, [(*i*-Pr-Xantphos)Pd(Ph)]$^+$Br$^-$, with the *i*-Pr-Xantphos ligand being in a P,O,P-coordination mode. For neutral and ionic forms of closely related Xantphos-type complexes, see, for example: (a) Kamer, P. C. J.; Van Leeuwen, P. W. N. M.; Reek, J. N. H. *Acc. Chem. Res.* **2001**, *34*, 895. (b) Zuideveld, M. A.; Swennenhuis, B. H. G.; Boele, M. D. K.; Guari, Y.; van Strijdonck, G. P. F; Reek, J. N. H.; Kamer, P. C. J.; Goubitz, K.; Fraanje, J.; Lutz, M.; Spek, A. L.; van Leeuwen, P. W. N. M. *Dalton* **2002**, 2308. (c) Koblenz, T. S.; Dekker, H. L.; De Koster, C. G.; Van Leeuwen, P. W. N. M.; Reek, J. N. H. *Chem. Commun.* **2006**, 1700.

(21) For reviews, see: (a) Brothers, P. J.; Roper, W. R. *Chem. Rev.* **1988**, *88*, 1293. (b) Torrens, H. *Coord. Chem. Rev.* **2005**, *249*, 1957. (c) Hughes, R. P. *Eur. J. Inorg. Chem.* **2009**, 4591.

(22) (a) Huang, D.; Caulton, K. G. *J. Am. Chem. Soc.* **1997**, *119*, 3185. (b) Huang, D.; Koren, P. R.; Folting, K.; Davidson, E. R.; Caulton, K. G. *J. Am. Chem. Soc.* **2000**, *122*, 8916.

(23) (a) Goodman, J.; Grushin, V. V.; Larichev, R. B.; Macgregor, S. A.; Marshall, W. J.; Roe, D. C. *J. Am. Chem. Soc.* **2009**, *131*, 4236. (b) Goodman, J.; Grushin, V. V.; Larichev, R. B.; Macgregor, S. A.; Marshall, W. J.; Roe, D. C. *J. Am. Chem. Soc.* **2010**, *132*, 12013.

(24) Appleton, T. G.; Hall, J. R.; Mathieson, M. T.; Neale, D. W. *J. Organomet. Chem.* **1993**, *453*, 307.

(25) Grushin, V. V. *Chem.—Eur. J.* **2002**, *8*, 1006.

(26) Fujita, K.; Yamashita, M.; Puschmann, F.; Martinez Alvarez-Falcon, M.; Incarvito, C. D.; Hartwig, J. F. *J. Am. Chem. Soc.* **2006**, *128*, 9044.

(27) Hamann, B. C.; Hartwig, J. F. *J. Am. Chem. Soc.* **1998**, *120*, 3694.

(28) Birkholz, M.-N.; Freixa, Z.; van Leeuwen, P. W. N. M. *Chem. Soc. Rev.* **2009**, *38*, 1099.

(29) Bakhmutov, V. I. *Practical NMR Relaxation for Chemists*; Wiley: Chichester, U.K., 2004.

(30) Unexpectedly, the T_1 times for both the cis and the trans isomers of **1** were *longer* in the presence of Xantphos: 10.7 vs 4.0 s for *cis*-**1** and 6.3 vs 3.2 s for *trans*-**1**. It is hardly conceivable that Xantphos, especially in such low amounts, could change dramatically the nature of the medium, lowering its viscosity, which would result in *faster* molecular reorientations of **1**. The T_1 effect observed could be more plausibly rationalized by paramagnetic species that are generated from **1** in the absence of Xantphos, but not in its presence. The CF_3—Ph reductive elimination from **1** occurs at as low as room temperature, albeit slowly (see above). In the presence of extra Xantphos, the unstable Pd(0) byproduct of this reaction, [(Xantphos)Pd], is efficiently stabilized in the form of [(Xantphos)$_2$Pd] (eq 1). As a result, only diamagnetic species are produced in the entire process. In the absence of extra Xantphos, however, [(Xantphos)Pd] decomposes (Scheme 2) to give rise to palladium colloids, which, unlike the bulk metal, exhibit ferromagnetic or near-ferromagnetic behavior.[31] Although these ferromagnetic species could not be detected by ESR, nor (considering their low concentration) by the Evans method,[32] their presence in the extra Xantphos-free solutions of **1** provides a rationale for the shortened relaxation times for both *cis*-**1** and *trans*-**1** (Table 2).

(31) (a) Taniyama, T.; Ohta, E.; Sato, T. *Europhys. Lett.* **1997**, *38*, 195. (b) Hori, H.; Teranishi, T.; Nakae, Y.; Seino, Y.; Miyake, M.; Yamada, S. *Phys. Lett. A* **1999**, *263*, 406. (c) Shinohara, T.; Sato, T.; Taniyama, T. *Phys. Rev. Lett.* **2003**, *91*, 197201. (d) Sampedro, B.; Crespo, P.; Hernando, A.; Litran, R.; Sanchez Lopez, J. C.; Lopez Cartes, C.; Fernandez, A.; Ramirez, J.; Gonzalez Calbet, J.; Vallet, M. *Phys. Rev. Lett.* **2003**, *91*, 237203. (e) Parolin, T. J.; Salman, Z.; Chakhalian, J.; Song, Q.; Chow, K. H.; Hossain, M. D.; Keeler, T. A.; Kiefl, R. F.; Kreitzman, S. R.; Levy, C. D. P.; Miller, R. I.; Morris, G. D.; Pearson, M. R.; Saadaoui, H.; Wang, D.; MacFarlane, W. A. *Phys. Rev. Lett.* **2007**, *98*, 047601. (f) Oba, Y.; Shinohara, T.; Oku, T.; Suzuki, J.-i.; Ohnuma, M.; Sato, T. *J. Phys. Soc. Jpn.* **2009**, *78*, 044711. (g) Oba, Y.; Okamoto, H.; Sato, T.; Shinohara, T.; Suzuki, J.; Nakamura, T.; Muro, T.; Osawa, H. *J. Phys. D* **2008**, *41*, 134024. (h) Teng, X.; Han, W.-Q.; Ku, W.; Hucker, M. *Angew. Chem., Int. Ed.* **2008**, *47*, 2055. (i) Xiao, C.; Ding, H.; Shen, C.; Yang, T.; Hui, C.; Gao, H.-J. *J. Phys. Chem. C* **2009**, *113*, 13466.

(32) (a) Evans, D. F. J. *J. Chem. Soc.* **1959**, 2003. (b) Live, D. H.; Chan, S. I. *Anal. Chem.* **1970**, *42*, 791. (c) Ostfeld, D.; Cohen, I. A. *J. Chem. Educ.* **1972**, *49*, 829. (d) Schubert, E. M. *J. Chem. Educ.* **1992**, *69*, 62.

(33) (a) Ananikov, V. P.; Musaev, D. G.; Morokuma, K. *Organometallics* **2005**, *24*, 715. See also (b) Sakaki, S.; Mizoe, N.; Musashi, Y.; Biswas, B.; Sugimoto, M. *J. Phys. Chem. A* **1998**, *102*, 8027.

(34) Calculations also probed the energetics of Pathway B, based on a sequence of α-F migration, Ph transfer onto the CF_2 ligand, and F—CF_2Ph coupling (see Scheme 1). An overall barrier of 26.1 kcal mol^{-1} was computed, with the highest-lying transition state corresponding to the Ph transfer step. Thus, calculations suggest that this mechanism may be competitive with direct reductive elimination; however, we rule out this process on the basis of the experimental studies carried out in excess water, which provided no evidence for a difluorocarbene intermediate. See the Supporting Information for full details.

(35) Anstaett, P.; Schoenebeck, F. *Chem. Eur. J.* **2011**, *17*, 12340. The transition state for CF_3—Ph reductive elimination from **cis-1** reported in this study exhibits less out-of-plane distortion than in **TS(cis-1 - 3)**, but was only slightly higher in energy when recomputed with the B97-D approach used here. In general, we found that the energy of the transition states and the precise ordering of the different transition-state structures varied subtly depending on whether dispersion effects were included in the calculation or not.

(36) Grimme, S. *J. Comput. Chem.* **2004**, *25*, 1463.

(37) (a) Sieffert, N.; Buehl, M. *Inorg. Chem.* **2009**, *48*, 4622. (b) Minenkov, Y.; Occhipinti, G.; Jensen, V. R. *J. Phys. Chem. A* **2009**, *113*, 11833. (c) McMullin, C. L.; Jover, J.; Harvey, J. N.; Fey, N. *Dalton Trans.* **2010**, *39*, 10833.

(38) Fey, N.; Ridgway, B. M.; Jover, J.; McMullin, C. L.; Harvey, J. N. *Dalton Trans.* **2011**, *40*, 11184.

(39) Dispersion effectscomputed with BLYP and B3PW91 employed Grimme's DFT-D3 setof parameters. See Grimme, S.; Antony, J.; Ehrlich, S.; Krieg, H. *J. Chem. Phys.* **2010**, *132*, 154104.

(40) Considering the small magnitude of the Xantphos effect and the k_{obs} determination error, the difference between the current (eq 4) and initial (Figure 7) concentration of Xantphos is ignored. This difference is even less important for the experiments using Xantphos in 5-, 10-, and 20-fold excess.

(41) Strictly speaking, our computational results indicate that $k_3 \neq 0$ (see Figure 5 and text above) and might be comparable to k_1 and k_5. The calculations also show, however, that **B** (**4**) is 15.8—18.5 kcal mol^{-1} higher in energy than **A** (**cis-1**) (Figure 4), suggesting that k_{-2} and k_4 are larger than k_1, k_3, and k_5. Therefore, the general kinetic equation (eq 4) may be simplified for two cases, as shown in the Supporting Information: (i) k_2 and k_{-4} are comparable to k_1, k_3, and k_5 (eq S1, Supporting Information) and (ii) k_2 and k_{-4} are smaller than k_1, k_3, and k_5 (eq S2, Supporting Information). Note that eq S2 is identical with eq 5 (Case 2).

(42) (a) There is another case that is kinetically indistinguishable from Cases 1 and 2: **C** does not produce $PhCF_3$ but decomposes via a different pathway during the reaction (Scheme S3, Supporting Information). The rate law for this scenario is presented in eq S5 (Supporting Information). This case is implausible, however, because of the high selectivity of the reaction that translates into the rate

constants k_{obs} derived from the appearance of $PhCF_3$ and from the disappearance of **1** being identical within the determination error. (b) Models omitting **B**, such as direct associative conversion of **A** to **C** in the presence of Xantphos (Scheme S1, Supporting Information) and, possibly, cis−trans isomerization of **C** (Scheme S2, Supporting Information), are not considered. The rate laws for these models (eqs S3 and S4, Supporting Information) include [XP] only in the numerators and not in the denominators, thereby failing to agree with the experimentally observed Xantphos effect.

(43) Naumann, D.; Kirij, N. V.; Maggiarosa, N.; Tyrra, W.; Yagupolskii, Y. L.; Wickleder, M. S. *Z. Anorg. Allg. Chem.* **2004**, *630*, 746.

(44) Asensio, G.; Cuenca, A. B.; Esteruelas, M. A.; Medio-Simon, M.; Olivan, M.; Valencia, M. *Inorg. Chem.* **2010**, *49*, 8665.

(45) Grushin, V. V. *Organometallics* **2000**, *19*, 1888.

(46) Binstead, R. A.; Zuberbühler, A.; Jung, B. *SPECFIT*, [3.0.34]; 2003.

(47) Frisch, M. J.; et al. *Gaussian 09*, revision A.02; Gaussian Inc.: Wallingford, CT, 2009.

(48) Grimme, S. *J. Comput. Chem.* **2006**, *27*, 1787.

(49) Andrae, D.; Haussermann, U.; Dolg, M.; Stoll, H.; Preuss, H. *Theor. Chim. Acta* **1990**, *77*, 123.

(50) Höllwarth, A.; Böhme, M.; Dapprich, S.; Ehlers, A. W.; Gobbi, A.; Jonas, V.; Köhler, K. F.; Stegmann, R.; Veldkamp, A.; Frenking, G. *Chem. Phys. Lett.* **1993**, *208*, 237.

(51) (a) Hehre, W. J.; Ditchfield, R.; Pople, J. A. *J. Chem. Phys.* **1972**, *56*, 2257. (b) Hariharan, P. C.; Pople, J. A. *Theor. Chim. Acta* **1973**, *28*, 213.

(52) Häller, L. J. L.; Page, M. J.; Erhardt, S.; Macgregor, S. A.; Mahon, M. F.; Naser, M. A.; Velez, A.; Whittlesey, M. K. *J. Am. Chem. Soc.* **2010**, *132*, 18408.